A Chemically Accurate Implicit-Solvent Coarse-Grained Model for Polystyrenesulfonate Solutions

RESEARCH · MAY 2015

DOI: 10.13140/RG.2.1.4516.6249

Macromolecules

Article

pubs.acs.org/Macromolecules

A Chemically Accurate Implicit-Solvent Coarse-Grained Model for Polystyrenesulfonate Solutions

Chunli Li,[†] Jiawei Shen,[‡] Christine Peter,[‡] and Nico F. A. van der Vegt*,[†]

[†]Center of Smart Interfaces, Technische Universität Darmstadt, Petersenstrasse 32, D-64287 Darmstadt, Germany

[‡]Max Planck Institute for Polymer Research, Ackermannweg 10, D-55128 Mainz, Germany

Supporting Information

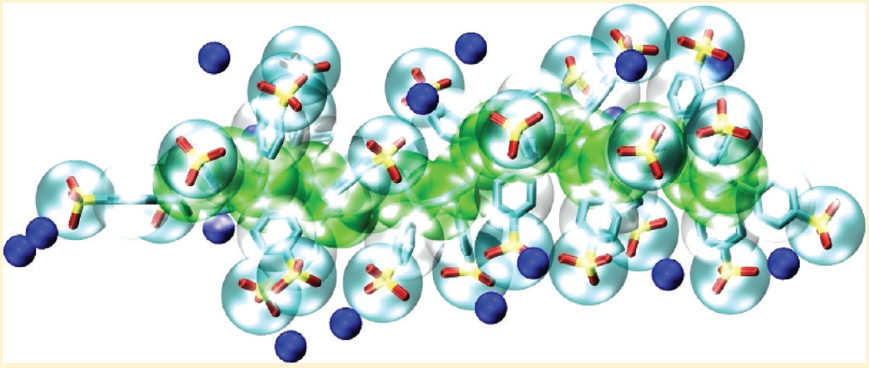

ABSTRACT: A systematic molecular coarse-graining (CG) approach for aqueous polyelectrolyte solutions is presented with sodium polystyrenesulfonate (NaPSS) with different chain tacticities as example systems. The styrenesulfonate repeat unit is mapped on a three-site CG representation with the counterion being modeled explicitly while the solvent is modeled implicitly. The CG force field discriminates between bonded and nonbonded forces, which have been developed independently. The bonded interactions correspond to the potentials of mean force of CG bond, angle, and torsion degrees of freedom obtained from sampling isolated chains with an atomistic force field that includes only the local interactions along the chain. The nonbonded interactions correspond to bead−bead potentials of mean force, obtained from simulations of small molecule or ion pairs in explicit water. The CG model reproduces the local and global conformations of polyelectrolyte chains in good agreement with the parent atomistic chains in aqueous solution. By using a relative dielectric permittivity based on the local concentration of counterions around the polyelectrolyte chain, the quality of our CG models can be further improved substantially. The effect of added salt (NaCl) on the radius of gyration of PSS chains with different tacticities has also been studied and results show the transferability of the CG NaPSS model to regimes with different electrostatic conditions. We furthermore show that the CG procedure presented here can easily be extended to CG models for partially sulfonated polystyrene systems.

1. INTRODUCTION

The structures and properties of polyelectrolyte systems are of great research interests due to their important role in biological systems and materials science.[1−7] In particular, many biopolymers such as proteins, DNA, and RNA are polyelectrolytes. Polyelectrolytes differ from low molecular weight electrolytes as well as from neutral polymers. They dissociate charges in polar solvents such as water and result in charged polymer chains and small mobile counterions.[8] The interplay between backbone hydrophobicity and electrostatic interactions from ionized groups results in an impressive variety of phenomena, which makes these systems very interesting from a fundamental point of view.

A considerable number of both experimental and theoretical studies have been performed to investigate the structure and dynamics of polyelectrolyte systems. For example, light scattering techniques have been widely used to study polyelectrolyte solutions, revealing properties such as the molecular weight, charge density, and concentrations of polyelectrolyte, along with the ionic strength and the pH of the solution,[9−14] as well as the formation of large multichain domains,[15,16] aggregates,[17] or clusters.[18] Detailed atomistic molecular dynamics (MD) studies of polyelectrolytes include investigations of poly(ethylene oxide) sulfonic acid in water,[19] the influences of counterions on DNA solvation in water,[20] simulations of poly(acrylic acid)with calcium counterions,[21] complex formations of PSS/PAA chains in water,[22] and surface effects on polyelectrolyte adsorption[23] etc. However, these simulations are rather expensive computationally due to the fact that polyelectrolyte chains, counterions, and/or water molecules in the systems are modeled explicitly. Limitations in terms of system sizes and time scales result in exhaustive sampling of

Received: November 11, 2011
Revised: February 2, 2012
Published: February 28, 2012

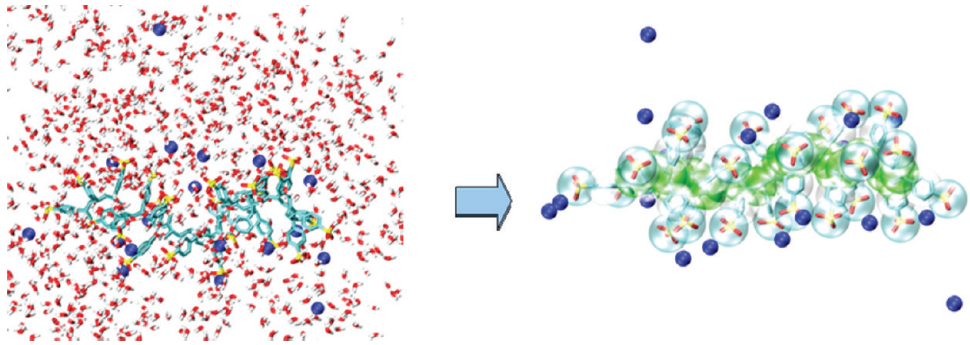

Figure 1. Implicit solvent CG model of a PSS chain with its counterions (Na^+) compared with its atomistic model. Left figure is the atomistic model, and right figure is the CG model. Small blue beads are counterions.

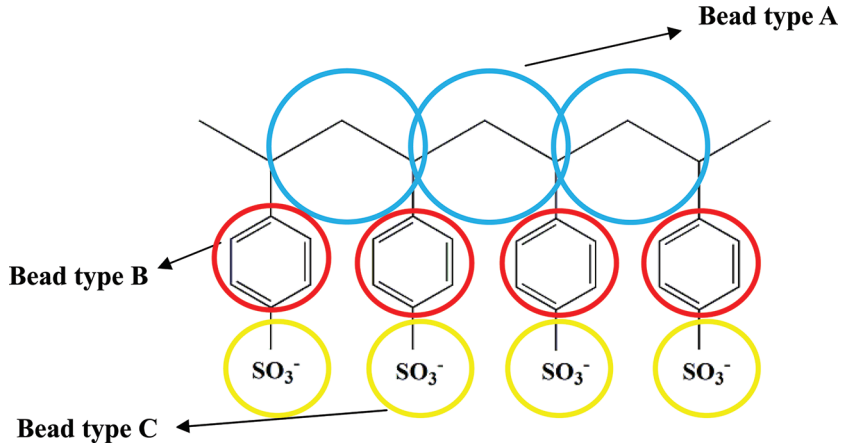

Figure 2. Mapping scheme of PSS chain.

polymer conformations only for short chains and/or few chains. On the other hand, coarse grained (CG) models have also been developed for polyelectrolyte solutions. However, some of these CG models use generic force fields, where polyelectrolytes with different chemical structures, counterions and co-ions, solvents and salt ions cannot be distinguished, ion specific effects and ion pairing with polymer side chains etc. cannot be indicated,[1,6,24] while in other CG models both water and counterions are represented implicitly; therefore, it is not possible to investigate ion correlation effects, such as the distributions of counterions along the polymer chain.[3]

In this work, a novel implicit solvent CG model was developed for a polyelectrolyte system containing a polystyrenesulfonate (PSS) chain with its counterions (Na^+) solvated in water. NaPSS was chosen due to its important applications in biomimetic materials research. In the development of synthetic bioinspired materials, NaPSS is widely used as the organic layer where nanometer-sized mineral particles are attached to generate hierarchically structured mesocrystal composites.[25] However, it is worth noting that the coarse graining strategy presented in this work can be easily extended to other polyelectrolyte systems as well.

In the CG model described here, the polymer chain and its counterions are both modeled explicitly while water molecules are modeled implicitly. Bonded and nonbonded CG potentials are obtained separately from independent atomistic level simulations. Furthermore, bonded interactions for NaPSS chains with different tacticities (isotactic, syndiotactic, atactic) are modeled differently in the CG description in analogy to a previously developed PS model.[26] Figure 1 depicts the resulting implicit solvent CG model compared with the parent atomistic model. By applying this strategy, we aim at developing a transferable CG model for polyelectrolyte solutions. In the results and discussion, the local and global conformational properties of CG isotactic, syndiotactic, atactic NaPSS chain in solutions are presented. The effects of added salt (NaCl) to the NaPSS solutions are also discussed and compared with atomistic level simulations. We point out that the CG models developed here can also be extended to systems containing NaPSS chains with various degrees of sulfonation.

2. COARSE GRAINING MODELS

2.1. Mapping Scheme. Each monomer of the PSS chain is mapped on three different CG bead types. The mapping scheme is shown in Figure 2. Bead A contains the CH_2 group in the backbone and half of its two neighboring CH groups to which the phenyl rings are attached; bead B contains all the atoms of the phenyl ring; and bead C contains all the atoms in the sulfonate group. All three beads are located at the center of mass of the group of atoms they contain. This mapping scheme leads to a CG PSS chain with alternating bead type A and B as backbone. CG bonds provide a "backbone" connectivity −A−B−A−B−. Bead C is attached to bead B as side group.

In the development of our CG model, PSS chains with different tacticities are distinguished by differentiating between two different scenarios of the stereochemistry in the subsequent monomers (diads) in the polymer chain. As shown in Figure 3, assuming the polymer backbone is in all-trans configuration, in a meso diad both phenyl rings point in the same direction while in a racemic diad phenyl rings point in opposite directions.

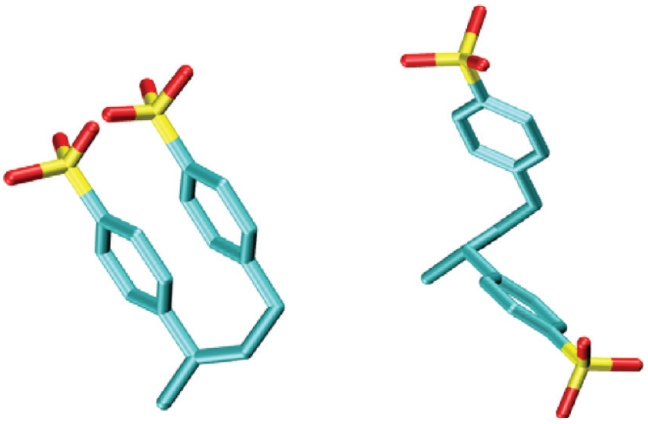

Figure 3. Diads in polystyrene: in meso diads (left), the subsequent side groups point in the same direction; in racemic diads (right), they point in opposite directions.

Correspondingly, a chain consisting of only meso diads is isotactic; a chain containing only racemic diads is syndiotactic; while in an atactic chain different types of diads are randomly distributed. More details about symmetry equivalent or analogous potentials (dihedrals) are discussed in the Supporting Information.

2.2. Coarse-Graining Procedure. Following the previous studies on the development of CG models for polystyrene (PS) chains,[26] our coarse-graining procedure is based on the same assumption that the total potential energy of a CG chain, U^{CG}, contains additive contributions of bonded, U^{CG}_{bonded}, and nonbonded, $U^{CG}_{nonbonded}$, terms:

$$U^{CG} = \sum U^{CG}_{bonded} + \sum U^{CG}_{nonbonded} \quad (1)$$

In this way, the CG bonded and nonbonded interaction potentials can be developed independently. In this work, the bonded potentials are derived from the atomistic sampling of an isolated PSS chain in vacuum,[26] while the nonbonded interactions are obtained by calculating the potentials of mean force (PMF) between two small molecules or ions in water representing the corresponding CG mapping beads in the polymer chain.[27]

2.2.1. Bonded Potentials. For the development of bonded potentials, atomistic MD simulations of isolated random walks in vacuum are performed at a selected temperature T. These simulations take into account the local bonded and nonbonded interactions between neighboring monomers on the chain while all nonbonded interactions between distant monomers are excluded.[26] The probability distributions of the CG bond lengths, $P^{CG}(r,T)$, bending angles, $P^{CG}(\theta,T)$ and dihedral angles, $P^{CG}(\phi,T)$, are obtained from the sampled trajectories and subsequently Boltzmann inverted to get the corresponding CG bond, angle and dihedral potentials of mean force:

$$U^{CG}(r, T) = -k_B T \ln(P^{CG}(r, T)/r^2) + C_r \quad (2)$$

$$U^{CG}(\vartheta, T) = -k_B T \ln(P^{CG}(\vartheta, T)/\sin\vartheta) + C_\vartheta \quad (3)$$

$$U^{CG}(\phi, T) = -k_B T \ln P^{CG}(\phi, T) + C_\phi \quad (4)$$

The probability distribution functions for the bond length and bond angle are normalized by taking into account the corresponding volume elements r^2 and sin θ. By means of this procedure we assume that the probability distributions $P^{CG}(r,\theta,\phi,T)$ obtained by the atomistic sampling of a single PSS chain random walk can be factorized as:

$$P^{CG}(r, \vartheta, \phi, T) = P^{CG}(r, T)P^{CG}(\vartheta, T)P^{CG}(\phi, T) \quad (5)$$

This assumption holds provided that the internal CG degrees of freedom are uncorrelated. However, previous studies show that correlations among internal CG degrees of freedom do exist in polystyrene models.[26,28,29] But by carefully choosing the range of local interactions along the backbone in the atomistic vacuum sampling and a suitable set of bonded interactions, correlations present in the atomistic models can be preserved in the CG models. Besides, the choice of CG mapping scheme is also crucial.

The distribution functions of the bonded degrees of freedom do not depend on long-range nonbonded interactions along the chain (or with other chains), nor on interactions with the solvent molecules or with counterions and salt ions. The net effect of these interactions on the chain conformations in solution depends on the thermodynamic conditions (concentration, temperature, *etc.*) and will be accounted for with independently developed nonbonded interactions that will be described in the next section.

It has been found that the interaction cutoff used in the single-chain sampling procedure critically determines whether the CG model is capable of reproducing conformational properties of the parent atomistic system down to the level of a few neighboring repeat units. This aspect will be discussed in greater detail below. The atomistic sampling run was performed with a single PSS chain (one isotactic and one syndiotactic chain) with 25 repeats units in vacuum at 298 K by using the stochastic dynamics integrator of GROMACS[30] with time coupling constant of 2 ps. By doing this we obtain all distribution functions necessary to model all tacticities. Force field parameters were taken from a united atom model presented by Hoda et al.[22] During the vacuum sampling, the electrostatic contributions to the potentials have been switched off. The effects of electrostatic interactions on the chain rigidity and conformations are separately accounted for through the nonbonded CG interactions discussed below.

2.2.2. Nonbonded Potentials. CG nonbonded potentials are obtained by calculating pair potentials of mean force as a function of distance between the mass centers of two small molecules or ions (representative of a CG bead) in a box of pure water. In this way, the molecules' internal degrees of freedom and the solvent degrees of freedom are accounted for implicitly in the effective bead−bead interactions. The resulting potentials thus depend explicitly on distance, but, as for the case of the bonded potentials, also contain an implicit dependence on state which limits the transferability of the model.

The potential of mean force between two molecules or groups in a box of pure water can be calculated from n distance constraint simulations by using the following equation:[27,31,32]

$$V_{PMF}(r) = \int_r^{r_m} \left[\langle f_c \rangle_s + \frac{2k_B T}{s} \right] ds + C \quad (6)$$

Here k_B is the Boltzmann constant, T is the temperature, f_c is the constraint force between the chosen centers of two molecules, and r_m is the maximum distance between the above two centers of molecules. For all PMF simulations in this

dx.doi.org/10.1021/ma202490h | *Macromolecules* 2012, 45, 2551−2561

research, the distance r varies from 0.2 to 1.2 nm in steps of 0.02 nm.

Previous studies[31] show that the effective potential between two ions in water is very close to a Coulomb interaction at distances greater than 1.0 nm. Therefore, we assume that beyond 1.2 nm, the PMF between two ions can be approximated with a Coulomb potential:

$$V_{PMF}(r) = \frac{q_1 q_2}{4\pi\varepsilon_0\varepsilon_r r}, \quad r > 1.2 \text{ nm} \tag{7}$$

where q_1 and q_2 are the charges of the ions, ε_0 is the dielectric permittivity of vacuum and ε_r is the relative dielectric permittivity of the solvent with a value of 72 for the SPC/E water model used in this work.[33] The constant C in eq 6 is equal to the Coulomb potential at 1.2 nm for the ion−ion interactions, and is chosen as identical zero for interactions between electrically neutral species. Furthermore, for the implementation of $V_{PMF}(r)$ in eq 6 and 7 in GROMACS, a short-range contribution $V_{short}(r)$ is obtained by subtracting the long-range Coulomb interaction between different molecules or ions from $V_{PMF}(r)$:

$$V_{short}(r) = V_{PMF}(r) - \frac{q_1 q_2}{4\pi\varepsilon_0\varepsilon_r r} \tag{8}$$

In our CG simulation, this short-range (non-Coulomb) contribution $V_{short}(r)$ is implemented in GROMACS in tabulated form, while the remaining long-ranged Coulomb interactions are computed using the particle mesh Ewald (PME) algorithm[34] with $\varepsilon_r = 72$.

In our PSS CG model, there are three different types of beads. Together with the counterions and co-ions, used to model effects of added salt, a total number of 15 bead−bead nonbonded pair potentials need to be constructed. Each of these potentials is obtained by calculating the PMF between a single pair of small molecules or ions in explicit water by means of eq 6. These small molecules or ions are chosen to represent the corresponding CG beads. Propane, benzene, and the methylsulfonate ion model the CG beads A, B, and C, respectively. The molecular centers used to define the distances in the constraint simulations were chosen to correspond to the mapping points of the CG PSS beads.

3. METHODS/COMPUTATIONAL DETAILS

The molecular dynamics package GROMACS 4.0.7 was used to perform all the simulations reported in this research.[30]

3.1. Atomistic MD Simulations. For the atomistic modeling of the NaPSS chain and sodium *p*-toluene sulfonate salt (the osmotic coefficient of this salt in water was later on calculated in order to validate the atomistic model), a united atom model based on the TraPPE force field was used.[5,22,35−37] The partial charges assigned on a PSS monomer are shown in Table 1. The force field parameters for the counterions (Na^+) and co-ions (Cl^-) was taken from ref 38. The SPC/E model[33] was used to model water molecules. All the bond lengths were constrained using the LINCS method[39] except those of water molecules, where the SETTLE algorithm[40] was used. For nonbonded interactions, a cutoff value of 1.0 nm was used for the van der Waals interaction. The PME method[40] was employed to treat Coulomb interactions, with a real space cutoff distance of 1.0 nm. A long-range dispersion correction was applied for energy and pressure. All atomistic simulations were performed under isothermal−isobaric (*NPT*) conditions. The Berendsen thermostat and barostat[41] was used to couple the system to an external bath at 1 bar and 298 K, with time coupling constants of 1 and 0.1 ps, respectively. The integration time step was 1 fs. We simulated NaPSS solutions of isotactic,

Table 1. Partial Charges Assigned on a PSS Monomer in the Atomistic Models and CG Models

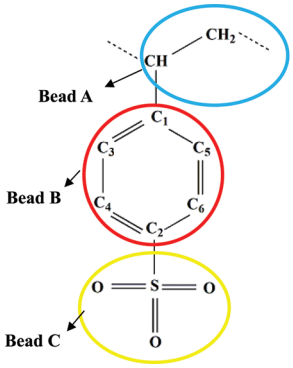

Atomistic		CG	
Group	Charge (e)	Group	Charge (e)
CH2/CH	0	A	0
C1	-0.03		
C2	-0.23	B	-0.505
C3/C5	-0.02		
C4/C6	-0.1025		
S	1.755	C	-0.495
O	-0.75		

syndiotactic, and atactic chains, respectively. Each system contained a single PSS chain with a degree of polymerization (DP) of 25 monomers, 25 Na^+ ions, and 13890 water molecules, which corresponds to a concentration of the polyions of 0.1 *m* (monomer). For systems where the effect of added salt was investigated, corresponding number of Na^+ and Cl^- ions were added.

The combination of the united atom PSS force field, ion and water models used in this work are validated by calculating the osmotic pressure of sodium *p*-toluene sulfonate solutions at different concentrations. The simulation system set up is depicted in Figure 4.[32,42] Two semipermeable walls are imposed perpendicular to the long axis z direction in a three-dimensional periodic simulation box, where salt ions are restricted in the central regions between two walls and water molecules can pass freely through the walls. A shifted 10−4 potential is set up so that ions experience repulsive forces as they start to diffuse out of the central region. By setting the simulation box to be semi-isotropic (*i.e.*, side length x and y are fixed while z is allowed to change) and performing *NPT* simulations, the osmotic pressure of the salt solutions can be calculated from the average forces exerted by the walls on the salt ions divided by the surface areas of two walls. In the above osmotic pressure calculations, 22224 water molecules were contained in each system; while 40, 80, 120, 160, and 200 ion pairs were used in the simulations for concentrations of sodium p-toluene sulfonate at 0.2, 0.4, 0.6, 0.8, and 1 *m* (molality) respectively. In each, 30 ns of *NPT* simulations were performed and the block average of the last 10 ns was used to calculate the osmotic pressure. Osmotic coefficients of the solutions were also calculated by using the following equation:

$$\phi = \frac{\pi}{CRT} \tag{9}$$

where φ is the osmotic coefficient, π is the osmotic pressure, C is twice the salt concentration in unit of mol/L, R is the universal gas constant, and T is the temperature, respectively.

3.2. Coarse-Grained MD Simulations. For all CG simulations presented in this work, bonded and nonbonded (short-range non-Coulomb) potentials are presented in tabulated forms implemented in GROMACS 4.0.7.[30] All CG simulations were performed in canonical (*NVT*) ensembles at 298 K by using stochastic dynamics with a time coupling constant of 2 ps.[30] Volumes of the CG systems were taken from the average volumes of their corresponding (*NPT*) atomistic systems. The integration time step is 4 fs and simulation time is 400 ns. In each CG system, a single PSS chain with DP = 25 or DP = 200 and the corresponding number of counterions (Na^+) were simulated. In systems investigating effects of added salt, certain numbers of salt ions (Na^+ and Cl^-) were added according to the salt concentrations. The mapping of atomistic models into CG beads was done by using the VOTCA toolkit.[43] The initial configurations of each CG system were taken from the mapping of the equilibrated structures from its corresponding atomistic simulations.

dx.doi.org/10.1021/ma202490h | *Macromolecules* 2012, 45, 2551−2561

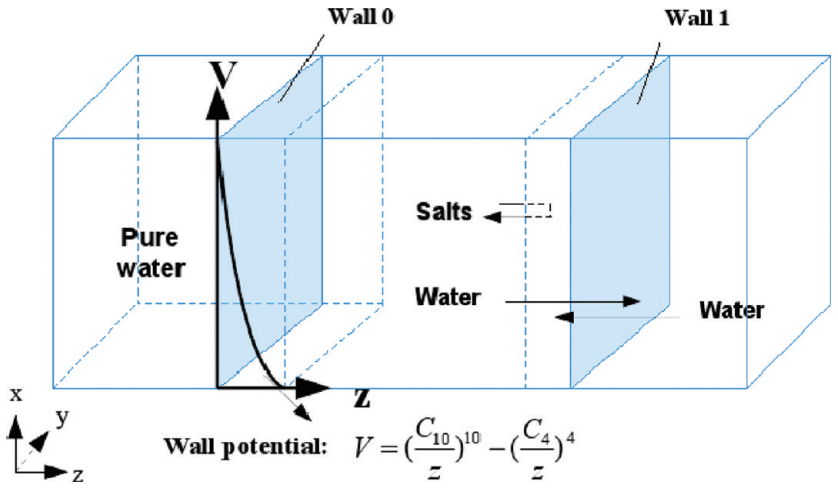

Figure 4. Simulation system set up[42] to calculate osmotic pressure of sodium *p*-toluene sulfonate solutions.

4. RESULTS AND DISCUSSION

4.1. Validation of Atomistic Models. Osmotic pressures and osmotic coefficients of sodium *p*-toluene sulfonate solutions were calculated at various concentrations, from 0.2 to 1 m, respectively. These results are compared with the experimental results and are shown in Figure 5. It can be seen

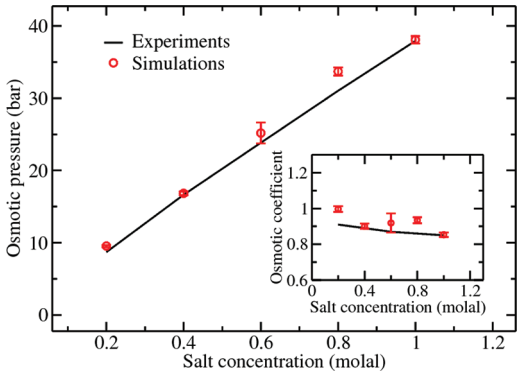

Figure 5. Comparison of simulation and experimental results for osmotic pressure and osmotic coefficient (inset) of sodium *p*-toluene sulfonate solutions at different concentrations (298 K).

that the united atom model we used here reproduces the experimental osmotic pressures[44] well at these concentrations. Therefore, the model has not been further refined and has been used as parent atomistic model for constructing the CG model by systematic coarse graining.

4.2. Development of CG Potentials. *4.2.1. Bonded Potentials.* The distributions of CG bond lengths, angles and dihedral angles depend on the "interaction range" used in the atomistic sampling of a single PSS chain in vacuum. Here, the "interaction range" refers to the number of neighboring beads (in terms of the CG mapping) that are included in evaluating the nonbonded pair interactions between atoms in atomistic vacuum simulations. The BAB angle distributions in fully isotactic and syndiotactic chains are shown in Figure 6 for different interaction ranges. We can see that in both cases the peak positions in the BAB angle distribution curves shift when local interactions up to 1−5 neighbors (the counting is done on the basis of CG beads) are included. With the inclusion of 1−6 interactions and beyond, the positions of the peaks always stay

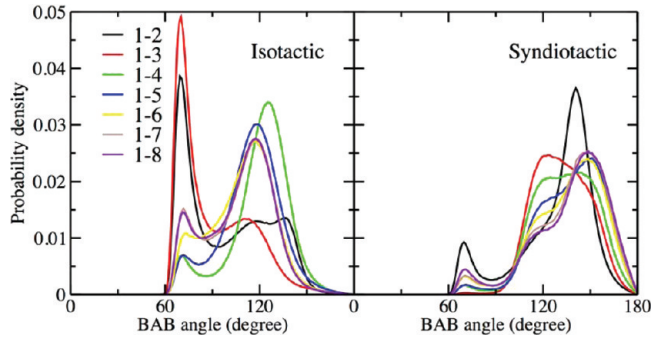

Figure 6. Distributions of BAB angles in a fully isotactic (left) and fully syndiotactic (right) single chain in vacuum at 298 K. The interaction range in these atomistic runs was varied from 1−2 to 1−8 in the CG description. All distributions are normalized.

the same, although their heights slightly change. By including the 1−5 interactions, the pentane effect in the polymer backbone is taken into account.

In order to further determine which range of intramolecular nonbonded interactions is required to fully represent the configurational sampling of the polymer chain, we looked at correlations between the probability distributions of two subsequent CG dihedral angles as shown in Figure 7. These plots show that more combinations of subsequent dihedral angles are suppressed as longer interaction ranges are included in the atomistic sampling of a single PSS chain in vacuum. But as 1−7 interactions are included, the correlation plot converges; i.e., no further changes are seen upon extending the range to 1−8 and beyond. This means that the interactions up to 1−7 determine the correlations and local conformations of a single PSS chain. Therefore, we performed the atomistic sampling of a single chain with all interactions included up to the 1−7 CG level for the derivation of the CG bond, angle, and dihedral angle potentials. However, we need to keep in mind that in this way, contributions from 1−5, 1−6, and 1−7 interactions are double counted since the final CG model uses additional nonbonded potentials for these interactions. The bonded potentials of the CG PSS model are summarized in the Supporting Information.

4.2.2. Nonbonded Effective Potentials. Figure 8 depicts the nonbonded potentials between different CG beads obtained from calculations of PMFs between molecules and/or ion pairs

dx.doi.org/10.1021/ma202490h | *Macromolecules* 2012, 45, 2551−2561

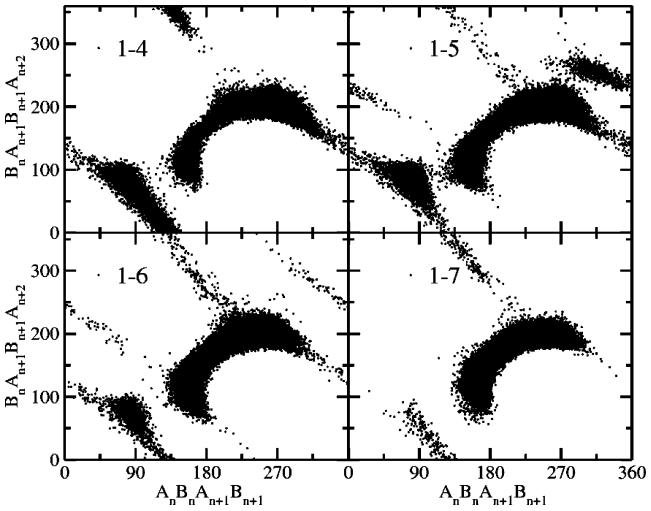

Figure 7. Conformation space sampled by two subsequent CG dihedral angles along the backbone in a single, isotactic chain obtained from atomistic sampling in vacuum (298 K). The two dihedrals share three beads, which form a BAB angle. Combinations with varied interaction ranges are shown.

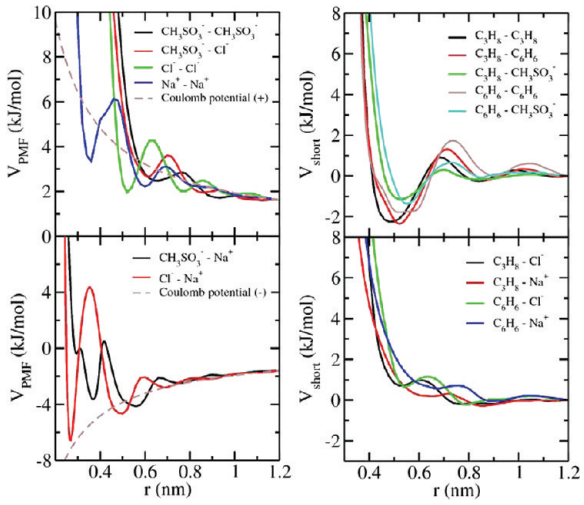

Figure 8. CG effective potentials obtained from PMF calculations: the left panel shows the $V_{PMF}(r)$ between ion pairs (compared with analytical Coulomb potentials), and the right panel shows the $V_{short}(r)$ between molecules/ion pairs without Coulomb interactions.

in water. The left panel in Figure 8 shows PMFs between ion pairs (compared with analytical Coulomb potentials), the right panel shows short-range potentials between molecules/ion pairs where Coulomb interactions are not involved. In this work, the obtained effective potentials, $V_{PMF}(r)$, are used to describe intermolecular interactions between CG beads, as well as for intramolecular interactions between beads that are separated by more than three CG bonds along the polymer chain. The nonbonded bead−bead pair potentials in Figure 8 include not only the effective, direct bead−bead interactions but also any changes in bead−solvent and solvent−solvent interactions as the two beads approach each other. As the beads perturb the local solvent structure in a way that may vary with the distance between them, the effective pair potentials contain solvation (or structural) contributions that give rise to the typical oscillations of the potentials at short-range. The effective interaction between oppositely charged beads (e.g., Na^+ with bead C or Na^+ with Cl^-) at contact distance corresponds to an energy minimum which is typically a factor 2 up to 3 times deeper than the effective (hydrophobic) interaction between the noncharged beads (A−A, B−B, or A−B) of the PSS chain.

We note that the short-range potentials involving the B bead have been obtained using benzene as a representative molecule, which, however, is electrically neutral unlike the phenyl unit of PSS, which carries a partial electronic charge of −0.505e (Table 1). The short-range potentials involving the C bead have in turn been obtained using methylsulfonate as a representative molecule, which carries a −1.0e charge, which compares to a −0.495e partial charge on the sulfonate group of PSS. While the coarse grained B and C beads both carry partial charges identical to those of the corresponding chemical groups of the polymer (giving rise to correct long-range electrostatic interactions), differences in the hydration structure of the small molecules and the chain fragments may give rise to deviations in the effective short-range interactions.

It is straightforward to extend the CG procedure presented here to PSS systems with varying degree of sulfonation. By virtue of the fact that the PMF calculations were performed between small molecules or ions instead of polymer segments, the development of CG potentials for partially sulfonated PS chains only requires the validation of the CG bonded part. In the Supporting Information, we compare the CG bonded potentials obtained from vacuum sampling of isolated atomistic chain of PSS, alternating styrenesulfonate and styrene groups, and PS respectively.

4.3. Comparison of Atomistic and CG Conformations.

As described in section 2.2, our CG bonded potentials are developed based on the random walk sampling of an isolated PSS atomistic chain in vacuum instead of that of PSS chain conformations in solution. Therefore, it is necessary to know how well the above CG potentials represent the atomistically sampled local conformations of the polyelectrolyte chain in aqueous solution. Our final CG model combines the bonded and nonbonded potentials discussed in the previous sections. Nonbonded interactions between beads on different chains and beads separated by more than three coarse grained bonds along the chain are described with the potentials summarized in Figure 8. Figure 9 shows the comparison of angle and dihedral

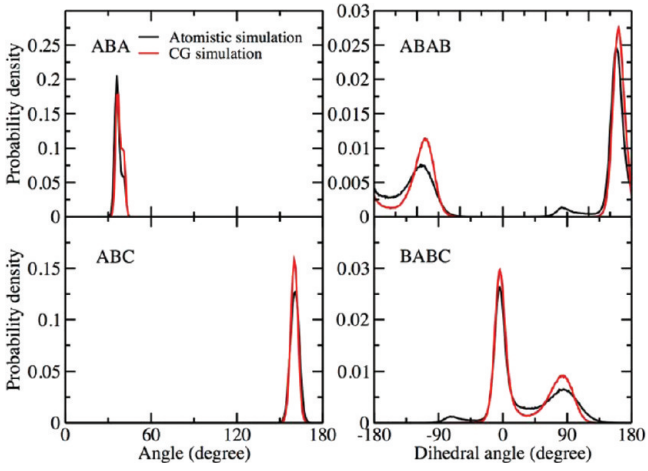

Figure 9. Distributions of selected CG degrees of freedom from atomistic (black curves) and CG (red curves). All figures shown here are calculations of a single isotactic PSS chain (DP = 25) with its counterions in water (298 K).

dx.doi.org/10.1021/ma202490h | *Macromolecules* 2012, 45, 2551−2561

distributions of an isotactic PSS chain in water with Na^+ counterions from atomistic and CG simulations, respectively. Bond distributions are always in perfect agreement and therefore not shown here. The simulation results of syndiotactic and atactic PSS solutions are reported in the Supporting Information. The agreement between the CG and atomistically sampled distributions is good; all major peaks observed in atomistic simulations are also shown in the CG simulations. Although some discrepancies can be observed in the dihedral distributions, the overall chain conformations are accurately reproduced as will be shown below. The BAB angle distributions (shown in the Supporting Information) of the CG atactic and isotactic systems show peak heights that deviate from the atomistic reference distributions. Introduction of a special 1−5 interaction results in better agreement (see Supporting Information).

Another important way to validate the CG model is to check to which extent the assumption of uncorrelated intramolecular degrees of freedom is realistic, and whether the CG model can preserve the correlations found in the atomistic sampling. To do this, correlations between two subsequent backbone dihedral angles were calculated and compared with the atomistic sampling in Figure 10. The comparison shows that

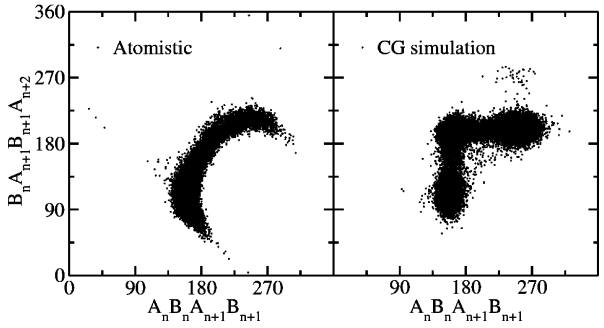

Figure 10. Conformation space of two subsequent CG dihedral angles along the backbone of an isotactic PSS chain in a system with its counterions in aqueous solution (298 K). Shown are results from atomistic and CG simulations.

the conformation space sampled by the atomistic and CG chains is quite similar, except for the regions around (160°, 200°). Most importantly, however, the CG model does not sample the region (270°, 90°) forbidden by the atomistic simulations. Hence, CG model reproduces the local correlations between adjacent torsional degrees of freedom along the PSS backbone in satisfactory agreement with the parent atomistic model.

The PSS chain conformations in CG and atomistic solutions can be compared by looking at $\langle R^2(n)\rangle$, the mean square distance between two monomers separated by n carbon−carbon bonds (two per monomer) along the backbone. To this end, the atomistic and CG simulation trajectories were analyzed using the mapping points of the A and B beads. Figure 11 shows $\langle R^2(n)\rangle$ of a single isotactic, syndiotactic and atactic PSS chain (DP = 25) in water. It can be seen that our CG model reproduces the mean square distance between internal monomers on chains with different tacticities in very good agreement with the atomistic model. In particular, the differences in $\langle R^2(n)\rangle$ for chains with different tacticities suggest that the stiffness of the isotactic, syndiotactic, and atactic chains is well reproduced in the CG model.

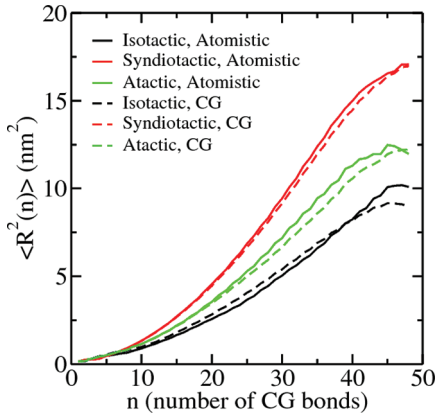

Figure 11. $\langle R^2(n)\rangle$, the mean square distance between two monomers separated by n bonds (two per monomer) along the backbone of a single isotactic, syndiotactic, and atactic PSS chain with DP = 25 monomers in salt free solution (298 K).

4.4. Counterion Distributions in Salt Free Solution. Primitive models for polyelectrolytes replace the aqueous solvent by a dielectric medium and introduce a constant dielectric permittivity in the description of electrostatic interactions. The resulting, attenuated Coulomb interaction is assumed to provide a realistic description independent of the separation distance between the charges. Hydration (or structural) forces, which start playing a role at the length scale of a few solvent diameters, are ignored in primitive models but accounted for in this work in the short-range part of the nonbonded interaction potential. Despite this sophistication, the *representability* and *transferability* of the new model needs to be investigated. Here, we investigate the counterion distribution around the PSS chain. Figure 12 shows that this quantity is not represented correctly by direct comparison with the explicit solvent atomistic model. The primitive CG model with $\varepsilon_r = 72$ does not reproduce the local structural features of the electrolyte in the atomistic explicit solvent system and shows an overall underprediction of the local counterion density. Because of the high negative charge density of the polyelectrolyte chain, the dielectric properties of its hydration water differ from bulk water as well as water molecules involved in mediating ionic interactions at the pair level. In previous, alternative developments of CG implicit solvent models, the representation of counterion distributions around the polyelectrolyte has been obtained with coarse graining procedures that iteratively improve a set of effective potentials until counterion distribution functions obtained from detailed atomistic simulations of polyelectrolyte solutions are reproduced.[46,47] Here, we follow a different route and investigate if representative and transferable potentials can be obtained by means of including a concentration dependent dielectric permittivity in the electrostatic pair forces as was introduced earlier by Hess et al.[31] Figure 12 compares the RDFs between the centers of mass of CG bead A, bead B, bead C, and Na^+ calculated from atomistic and CG simulations, respectively. The CG model, which uses a Na^+-chain interaction potential based on pair PMFs obtained at infinite dilution of ions (eqs 6−8) and a dielectric constant of 72, reproduces the positions of the peaks in the RDF curve, but underestimates the heights of the peaks. Because of the strong electrostatic interactions between the polyelectrolyte charges and its counterions, the local concentration of Na^+ close to PSS chain is much higher than at

dx.doi.org/10.1021/ma202490h | *Macromolecules* 2012, 45, 2551−2561

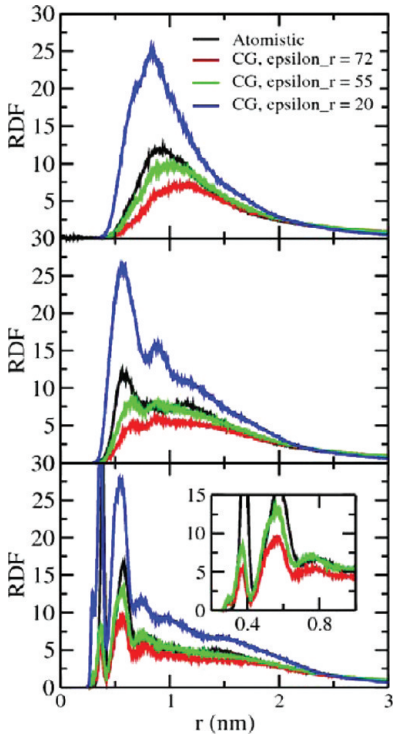

Figure 12. Comparison of RDFs between the center of mass of CG bead A (top panel), bead B (middle panel), bead C (lower panel), and Na^+ obtained from atomistic simulation, CG simulation with ε_r = 72, CG simulation with ε_r = 55, and CG simulation with ε_r = 20.

infinite dilution of ions where the pair potential was developed. This large, local increase of charge concentration leads to significant electrostriction of water, a resulting decrease of the local dielectric permittivity and increase of the electrostatic forces. To estimate the reduction of the dielectric permittivity, we evaluated the local concentration of Na^+ ions around a PSS chain by counting the total number of Na^+ ions in the first and second peaks of atomistic RDF between bead C and Na^+ and dividing it by the volume occupied by these Na^+ ions. In this case, the concentration is about 1 *m*. The resulting dielectric permittivity (ε_r = 55) was obtained by calculating the fluctuations of the total solvent dipole moment[45] in atomistic simulations of a 1 *m* of sodium *p*-toluene sulfonate solution. CG simulations were performed with a dielectric permittivity of 55 and the resulting RDF between different CG beads and Na^+ ions are shown in Figure 12. It shows that by using a concentration dependent relative dielectric permittivity, the CG RDF curves are substantially improved. In particular, the second peak and the long-range tail of the RDF curve between bead C and Na^+ agree very well with the atomistic curves. However, the improvement in the first peaks of all curves is still limited, which may be owing to limitations of the short-range potentials (see section 4.2.2). To see if further improvement could be achieved, we performed CG simulations with even smaller values of relative dielectric permittivity. The bottom graph in Figure 12 shows the RDF between bead C and Na^+ ions with ε_r = 20. It can be seen that with ε_r = 20, the height of the first peak is reproduced. However, the RDF of the coarse grained system is overstructured everywhere else, and moreover shows a shoulder at small distance before the first peak in the atomistic RDF. The A−Na^+ (Figure 12, top) and B−Na^+ (Figure 12, middle) RDFs obtained with ε_r = 20 are also severely overstructured. This leads us to the conclusion that the physically motivated ε_r = 55 indeed gives a very good representation of the screened electrostatics of the polyelectrolyte/counterion system.

The approach followed here provides a good representation of the counterion distribution at all distances except direct ion-polyelectrolyte contact. Although perfect agreement with atomistic simulation data has not been reached, the use of a concentration dependent dielectric constant bears a significant advantage, since it offers a route to ensure transferability of the effective pair potential to systems with different electrostatic conditions (*e.g.*, added salt) as was illustrated in our previous work on simple electrolyte solutions.[32] The comparison with atomistic simulation data in Figure 12 clearly demonstrates that the polyelectrolyte chain-counterion interactions obtained from the primitive CG model with ε_r = 72 are significantly too weak.

4.5. Effective Charges. In polyelectrolyte solutions, condensation of oppositely charged counterions on the polyelectrolyte chain can greatly affect the conformations of the chains. To describe the local distribution of Na^+ ions along the PSS chain, effective charges on beads of the PSS chain were calculated.[24] To this end, we calculated the distributions of distances between each monomer and the counterions:

$$n_q(r, j) = \langle \sum_{i \in C_j} \upsilon_i \delta(r - d_i(j)) \rangle \tag{10}$$

Here, $n_q(r,j)$ is the canonical average (over the simulation trajectory) of ion charge located at distance r from the charged monomer j. For each simulation configuration the counterions are attributed to their respective closest monomer j; C_j denotes the set of all counterions i to which monomer j is the closest monomer of the chain; ν_i is the charge on counterion i; $d_i(j)$ is the distance between the counterion i and its closest charged monomer j; and $\delta(x)$ is the Dirac delta function.

The local effective charge is then defined as

$$q_{eff}(r, j) = \nu(j) + P(r, j) \tag{11}$$

where ν_j is the charge on monomer j, and $P(r,j)$ is the local ion charge contained in the interval $[0, r]$ by integrating $n_q(r,j)$ from zero to r:

$$P(r, j) = \int_0^r \mathrm{d}r' n_q(r', j) \tag{12}$$

In our systems, due to the fact that CG bead B and C both carry charges, effective charges were calculated relative to beads B and C. Figure 13 shows the effective charges on bead B and C along the contour length of the PSS chain (DP=25) with ε_r = 55. The effects of ε_r values on the results of effective charges will be discussed later. For the effective charges on bead B, the cutoff radius for the integration in eq 12 was chosen to be the distance corresponding to the minimum between the first and second peak in the B - Na^+ RDF (0.76 nm); while for the effective charges on bead C, the minimum between the first and second, and between the second and third peak of C−Na^+ RDF curve were chosen as the cutoff distances (0.42 and 0.66 nm), respectively. In agreement with the observation of Limbach et al.[24] on a generic model of polyelectrolyte solution, the choice of the cutoff radius does not affect the qualitative form of the effective charge curves. The effective charges on beads C and B, obtained from CG simulations, are in very good agreement with the corresponding data from the detailed atomistic simulations for cutoff radii of 0.66 and 0.76 nm, respectively.

dx.doi.org/10.1021/ma202490h | *Macromolecules* 2012, 45, 2551−2561

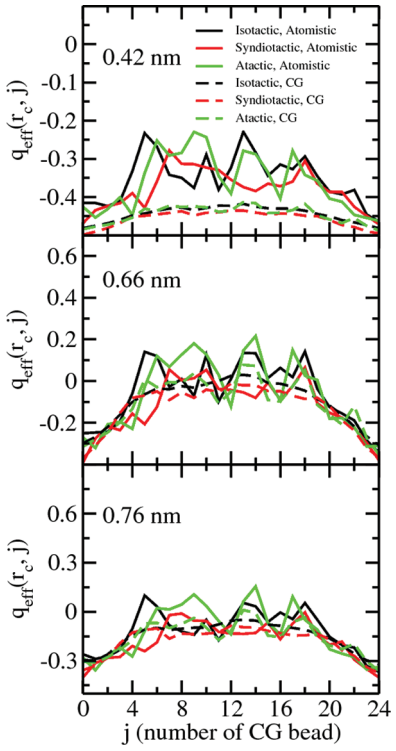

Figure 13. Effective charges on bead C (top and middle panel with cutoff radii 0.42 and 0.66 nm, respectively) and bead B (lower panel, cutoff radius 0.76 nm) of PSS chains (DP = 25) in water obtained from simulations (298 K) with ε_r = 55.

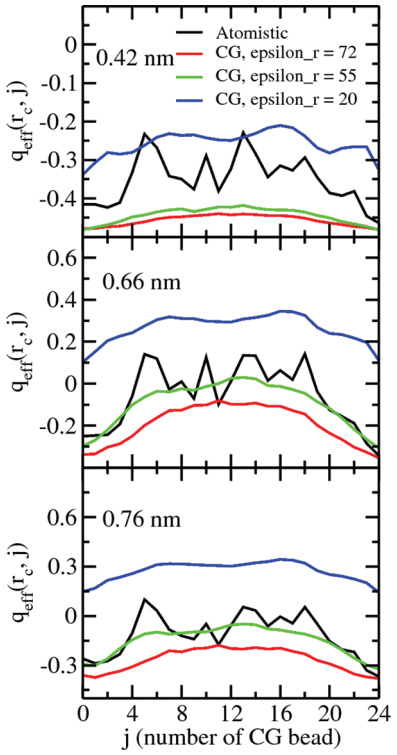

Figure 14. Effective charges of the isotactic PSS chain (DP = 25) obtained from atomistic simulations and CG simulations (298 K) with relative dielectric permittivities of 72, 55, and 20. The data in the top and middle panels correspond to the effective charge on bead C, the data in the lower panel corresponds to the effective charge on bead B.

Only for the short cutoff radius of 0.42 nm (bead C), the effective charge is overpredicted which is due to the discrepancy in the local electrolyte structure (see Figure 12). Inhomogeneity of effective charges along the contour length is observed both in atomistic and CG simulations, with beads in the central part of the backbone being stronger screened than those at the chain ends. This is due to the higher charge density of the central part of the polyelectrolyte backbone. Atomistic effective charge curves show rather big fluctuations due to the poor statistics, and no obvious differences can be identified among PSS chain with different tacticities. Comparing with atomistic simulation results, CG simulation curves are much smoother, except that the atactic chain exhibits relatively larger fluctuations. These larger fluctuations may derive from the inhomogeneous distributions of meso and racemic diads along the atactic PSS chain.

In Figure 14, it is again shown that the agreement of the effective charge is strongly dependent on the value of the concentration dependent dielectric permittivity. The different lines represent the effective charges on beads of the isotactic PSS chain obtained from atomistic simulations and CG simulations with relative dielectric permittivity of 72, 55, and 20 respectively. The dielectric permittivity of 55 gives the best agreement (except for bead C at very short cutoff radius, due to the deviation of the local structure as discussed above). Note that the difference between ε_r = 20 and ε_r = 55 and larger is qualitative. At ε_r = 20 the system is overcharged and the absolute sign of the charge is inverted, i.e. the beads appears to be positively charged instead of negatively.

4.6. PSS Conformations in Solution with Added Salt. In salt free solution, the PSS chain is expanded due to electrostatic repulsion among negatively charged groups on different monomers. On the other hand, counterions prefer to condense on the chain thereby reducing its net charge and consequently facilitating chain contraction. The presence of small molecular monovalent salts has long been known to enhance this condenstation effect.[48,49] Therefore, by adding salt (for example NaCl) to the polyelectrolyte solution, we expect a shrinkage of the polyelectrolyte chain dimension.

We characterize the polyelectrolyte conformation by its radius of gyration (R_g) and compare R_g of the PSS chains calculated from atomistic and CG simulations. In the CG simulations, the relative dielectric permittivity ε_r was chosen to be 72, 57.50, and 50.70 for systems with NaCl concentration of 0, 1, and 2 *m*, respectively. These values were obtained by calculating the fluctuations of the total solvent dipole moment of NaCl solutions at corresponding concentrations. Here, in order to identify the effects of added salt only, the above ε_r values were not further adjusted according to the local concentrations of Na^+ ions around the PSS chain in each atomistic system. In fact, we also investigated the effects of changing ε_r on the change of R_g of the isotactic PSS chain in salt free solution. We found that by decreasing ε_r, R_g of the isotactic PSS chain slightly decreases (shown in Figure 15), in agreement with the observations in the RDF curves in Figure 12.

The radius of gyration of PSS chains with different tacticities obtained from both atomistic and CG simulations are shown in Figure 15. The atomistic and CG simulations both show the order R_g (syndiotactic) > R_g (atactic) > R_g (isotactic) in solutions with or without added salt. With the addition of salt, R_g of PSS chains with different tacticities decreases, showing the trend of the polymer chain contraction due to salt-induced

dx.doi.org/10.1021/ma202490h | *Macromolecules* 2012, 45, 2551–2561

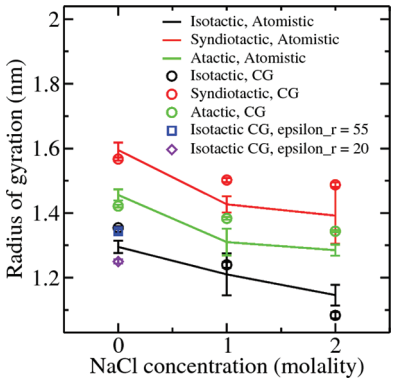

Figure 15. Effect of added salt on the radius of gyration (R_g) of the polyelectrolyte chain (DP = 25) with different tacticities solvated in water with its counterions (298 K).

screening of the electrostatic interactions. As mentioned above, in the systems with added NaCl, salt concentration dependent dielectric permittivity parameters were used to take into account different multibody effects in polyelectrolyte solutions with different salt concentrations. Without having to derive a new model at each salt concentration, our CG model can reasonably reproduce R_g values of PSS chains with different tacticities over a range of salt concentrations, showing the transferability of the CG model upon salt conditions.

4.7. Chemical Accuracy of the CG Model: Counterion Distributions around Isotactic and Syndiotactic NaPSS Chains (DP = 200). The PSS coarse grained model has been developed with an eye to chemical and thermodynamic transferability. The model allows for variation of the chain length, tacticity, degree of sulfonation and electrolyte concentration. A detailed study of how polyelectrolyte properties depend on such variations goes beyond the scope of the present work. Here, we examine one aspect of the chemical accuracy of the CG model, which is not represented by generic polyelectrolyte models. Figure 16 (upper panel) shows the effective charges of the C beads (within 0.66 nm radius) of isotactic and syndiotactic PSS chains with DP=200 in salt-free and 0.1 *m* salt (NaCl) solutions. In agreement with the data for shorter chains in Figure 13, the central beads of the chain are always screened more strongly by the counterions than the outer beads. In 0.1 *m* NaCl solution, the effective charges of all C beads on the isotactic chain are further screened, leading to an almost complete charge neutralization of these beads. Interestingly, the effective charges of inner C beads of the syndiotactic chain are hardly affected by salt, while the outer beads' effective charges increase (becomes more strongly negative)—rather than decrease − in 0.1 *m* salt solution. The Cl^- co-ions do not play a role in the observed effect, as they were found to always stay far away from the polyelectrolyte chain. In moving from salt free conditions to 0.1 *m* NaCl, the Na^+ counterions however redistribute around the polyelectrolyte chain in a decisively different manner for the two stereoregular polyelectrolytes. Figure 16 (lower panel) shows the Na^+ ion concentration vicinal to C beads of the isotactic and syndiotactic PSS chains in salt free solution and in 0.1 *m* NaCl. For the isotactic system, the Na^+ ion concentration vicinal to C beads increases monotonically relative to the salt free system over the entire distance range. This is in agreement with the observed charge screening of the C beads in the upper panel of Figure 16. We however observe that the local Na^+ ion

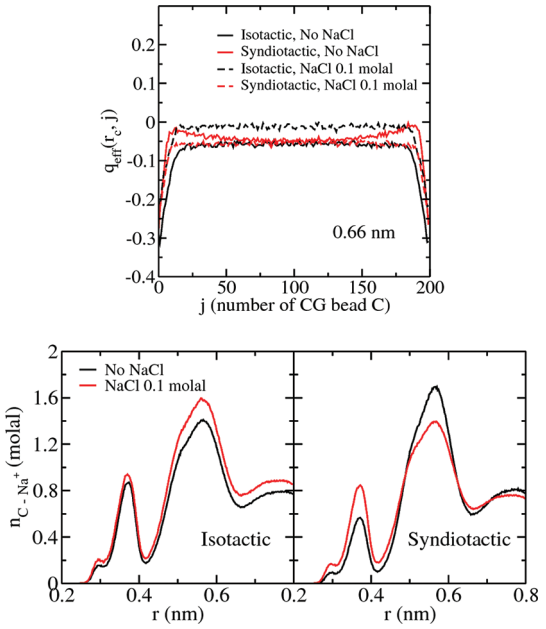

Figure 16. Effective charges within cutoff radius of 0.66 nm on the C bead of PSS (DP = 200) in salt-free and 0.1 *m* NaCl salt solution (upper panel). Comparison of the local number density of Na^+ ions at the distance *r* from beads C on isotactic and syndiotactic polyelectrolyte chains (lower panel).

concentration around C beads on the syndiotactic chain increases at small distances (<0.47 nm) but decreases at larger distances (>0.50 nm) with the addition of NaCl. Thus, upon increasing salt, the effective negative charge of the C bead increases within the range of 0.66 nm, despite stronger *direct* charge screening through Na^+ contact pair interactions (<0.47 nm) with the C beads on the syndiotactic chain. It is furthermore noteworthy that comparison of the local Na^+ ion concentration for isotactic and syndiotactic PSS in salt free solution clearly indicates that the counterions around syndiotactic PSS have stronger preference to accumulate in the second peak (~0.57 nm) while a larger fraction of the counterions around the isotactic chain accumulate in the first peak and form direct contact interactions with the C beads. This behavior is likely caused by a larger charge density of the isotactic chain. The BAB angle of the isotactic chain is smaller than the corresponding angle of the syndiotactic chain (see Figures S5 and S6 in the Supporting Information), which causes smaller distances among adjacent C beads in the isotactic chain and a correspondingly larger charge density. Consequently, both the chemically accurate representation of the chain conformations and the locally specific and transferable behavior of the ion−ion interaction are crucial to observe such an effect in the CG model.

5. CONCLUSIONS

In conclusion, we have developed a chemically and thermodynamically transferable coarse grained PSS model allowing for systematic variation of chain length, tacticity, electrolyte concentration and degree of sulfonation with high chemical accuracy and a close link to the parent atomistic model. The model features an implicit solvent (water) representation, while both the polyelectrolyte chain and its counterions are modeled explicitly. The short-range chemical forces related to ionic solvation are taken into account and

dx.doi.org/10.1021/ma202490h | *Macromolecules* 2012, 45, 2551−2561

specific-ion phenomena can therefore be investigated. CG bonded and nonbonded potentials are developed separately, where bonded potentials are obtained from atomistic sampling of random walks of a single polyelectrolyte chain in vacuum and nonbonded potentials are developed from the calculation of pair PMFs between two small molecules or ions in water representing corresponding CG beads. Comparison of distributions of CG bonded degrees of freedom and internal distances along the polymer chain show that the resulting CG model reproduces the atomistically sampled local conformation of a PSS chain (with 25 monomers) in solution with different tacticities. Our CG model also reproduces the positions of the peaks in the atomistic radial distribution function (RDF) curve between PSS chain beads and Na^+, although the heights of the peaks are underestimated. Furthermore, by adjusting the dielectric permittivity based on the local concentration of counterions around the polyelectrolyte chain, the CG RDF curve is substantially improved and reproduces the counterion structure around the chain (except for very local effects) very well. This observation shows that with primitive polyelectrolyte model (solvent dielectric permittivity $\varepsilon_r = 72$), the interactions between counterions and the polyelectrolyte chain calculated by CG models are too weak compared with atomistic models. Effects of adding salt on the change of radius of gyration of PSS chains with different tacticities were also studied. The agreement of CG model and atomistic simulations on R_g values show the transferability of our CG model upon salt conditions, even without having to rederive new potentials at each different salt concentration.

■ ASSOCIATED CONTENT

Ⓢ Supporting Information

Coarse graining models, polyelectrolyte solution simulations, and partially sulfonated polystyrene CG models. This material is available free of charge via the Internet at http://pubs.acs.org.

■ AUTHOR INFORMATION

Corresponding Author

*E-mail: vandervegt@csi.tu-darmstadt.de.

Notes

The authors declare no competing financial interest.

■ ACKNOWLEDGMENTS

We would like to thank Dominik Fritz and Kurt Kremer for many helpful discussions. This project has been carried out as part of the priority program SPP 1420 by the German Science Foundation. C.P. gratefully acknowledges financial support by the German Science Foundation within the Emmy Noether program (grant PE 1625/1).

■ REFERENCES

(1) Limbach, H. J.; Holm, C. *J. Phys. Chem. B* **2003**, *107*, 8041.
(2) Carrillo, J. M. Y.; Dobrynin, A. V. *J.Phys.Chem. B* **2010**, *114*, 9391.
(3) Reith, D.; Mueller, B.; Mueller-Plathe, F.; Wiegand, S. *J. Chem. Phys.* **2002**, *116*, 9100.
(4) Essafi, W.; Lafuma, F.; Baigl, D.; Williams, C. E. *Europhys. Lett.* **2005**, *71*, 938.
(5) Vishnyakov, A.; Neimark, A. V. *J. Chem. Phys.* **2008**, *128*, 164902.
(6) Kalyuzhnyi, Y. V.; Vlachy, V.; Cummings, P. T. *Chem. Phys. Lett.* **2007**, *438*, 238.
(7) Stevens, M. J.; Plimpton, S. J. *Eur. Phys. J. B* **1998**, *2*, 341.
(8) Barrat, J. L.; Joanny, J. F. *Adv. Chem. Phys.* **1996**, *94*, 1.
(9) Sedlak, M. *Langmuir* **1999**, *15*, 4045.
(10) Xia, J.; Dubin, P. L.; Edwards, S.; Havel, H. *J. Polym. Sci., Part B: Polym. Phys.* **1995**, *33*, 1117.
(11) Tanahatoe, J. J.; Kuil, M. E. *J. Phys. Chem. B* **1997**, *101*, 9233.
(12) Chisaka, S.; Norisuye, T. *J. Polym. Sci., Part B: Polym. Phys.* **2001**, *39*, 2071.
(13) Pohlmeier, A.; Haber-Pohlmeier, S. *J. Colloid Interface Sci.* **2004**, *273*, 369.
(14) Zhou, K.; Li, J.; Lu, Y.; Zhang, G.; Xie, Z.; Wu, C. *Macromolecules* **2009**, *42*, 7146.
(15) Sedlak, M. *J. Chem. Phys.* **2002**, *116*, 5236.
(16) Sedlak, M. *J. Chem. Phys.* **2005**, *122*, 151102.
(17) Michel, R. C.; Reed, W. F. *Biopolymers* **2000**, *53*, 19.
(18) Smits, R. G.; Kuil, M. E.; Mandel, M. *Macromolecules* **1994**, *27*, 5599.
(19) Ennari, J.; Elomaa, M.; Sundholm, F. *Polymer* **1999**, *40*, 2001.
(20) Lyubartsev, A. P.; Laaksonen, A. *J. Biomol. Struct. Dyn.* **1998**, *16*, 579.
(21) Duca, J. S.; Hopfinger, A. J. *Comput. Theor. Polym. Sci.* **1999**, *9*, 227.
(22) Hoda, N.; Larson, R. G. *Macromolecules* **2009**, *42*, 8851.
(23) Qiao, B. F.; Cerda, J. J.; Holm, C. *Macromolecules* **2011**, *44*, 1707.
(24) Limbach, H. J.; Holm, C. *J. Chem. Phys.* **2001**, *114*, 9674.
(25) Coelfen, H.; Antonietti, M. *Angew. Chem., Int. Ed.* **2005**, *44*, 5576.
(26) Fritz, D.; Harmandaris, V. A.; Kremer, K.; van der Vegt, N. F. A. *Macromolecules* **2009**, *42*, 7579.
(27) Villa, A.; Peter, C.; van der Vegt, N. F. A. *Phys. Chem. Chem. Phys.* **2009**, *11*, 2077.
(28) Harmandaris, V. A.; Adhikari, N. P.; van der Vegt, N. F. A.; Kremer, K. *Macromolecules* **2006**, *39*, 6708.
(29) Harmandaris, V. A.; Reith, D.; van der Vegt, N. F. A.; Kremer, K. *Macromol. Chem. Phys.* **2007**, *208*, 2109.
(30) Hess, B.; Kutzner, C.; van der Spoel, D.; Lindahl, E. *J. Chem. Theory Comput.* **2008**, *4*, 435.
(31) Hess, B.; Holm, C.; van der Vegt, N. F. A. *Phys. Rev. Lett.* **2006**, *96*, 147801.
(32) Shen, J.; Li, C.; van der Vegt, N. F. A.; Peter, C. *J. Chem. Theory Comput.* **2011**, *7*, 1916.
(33) Berendsen, H. J. C.; Grigera, J. R.; Straatsma, T. P. *J. Phys. Chem.* **1987**, *91*, 6269.
(34) Darden, T.; York, D.; Pedersen, L. *J. Chem. Phys.* **1993**, *98*, 10089.
(35) Wick, C. D.; Martin, M. G.; Siepmann, J. I. *J. Phys. Chem. B* **2000**, *104*, 8008.
(36) Martin, M. G.; Siepmann, J. I. *J. Phys. Chem. B* **1999**, *103*, 4508.
(37) Vishnyakov, A.; Neimark, A. *J. Phys. Chem. B* **2000**, *104*, 4471.
(38) Hess, B.; van der Vegt, N. F. A. *Proc. Natl. Acad. Sci. U.S.A.* **2009**, *106*, 13296.
(39) Hess, B.; Bekker, H.; Berendsen, H. J. C.; Fraaije, J. G. E. M. *J. Comput. Chem.* **1997**, *18*, 1463.
(40) Miyamoto, S.; Kollman, P. A. *J. Comput. Chem.* **1992**, *13*, 952.
(41) Berendsen, H. J. C.; Postma, J. P. M.; van Gunsteren, W. F.; DiNola, A.; Haak, J. R. *J. Chem. Phys.* **1984**, *81*, 3684.
(42) Luo, Y.; Roux, B. *J. Phys. Chem. Lett.* **2010**, *1*, 183.
(43) Ruehle, V.; Junghans, C.; Lukyanov, A.; Kremer, K.; Andrienko, D. *J. Chem. Theory Comput.* **2009**, *5*, 3211.
(44) Robinson, R. A.; Stokes, R. H. *Trans. Faraday Soc* **1949**, *45*, 612.
(45) Neumann, M. *Mol. Phys.* **1983**, *50*, 841.
(46) Savelyev, A.; Papoian, G. A. *J. Phys. Chem. B* **2009**, *113*, 7785.
(47) Savelyev, A.; Papoian, G. A. *Proc. Natl. Acad. Sci. U.S.A.* **2010**, *107*, 20340.
(48) Manning, G. S. *J. Chem. Phys.* **1969**, *51*, 924.
(49) Kundagrami, A.; Muthukumar, M. *J. Chem. Phys.* **2008**, *128*, 244901.